

In vivo fluorescent imaging of the mouse retina using adaptive optics

David P. Biss, Daniel Sumorok, Stephen A. Burns, and Robert H. Webb

Schepens Eye Research Institute, 20 Staniford Street, Boston, Massachusetts 02114, USA

Yaopeng Zhou and Thomas G. Bifano

Boston University, 15 St. Mary Street, Brookline, Massachusetts 02446, USA

Daniel Côté, Israel Veilleux, Parisa Zamiri, and Charles P. Lin

Advanced Microscopy Program, Wellman Center for Photomedicine, Massachusetts General Hospital, Harvard Medical School, 185 Cambridge Street, Boston, Massachusetts 02114, USA

Received September 14, 2006; revised December 1, 2006; accepted December 12, 2006;
posted December 15, 2006 (Doc. ID 75051); published February 15, 2007

In vivo imaging of the mouse retina using visible and near infrared wavelengths does not achieve diffraction-limited resolution due to wavefront aberrations induced by the eye. Considering the pupil size and axial dimension of the eye, it is expected that unaberrated imaging of the retina would have a transverse resolution of $2\ \mu\text{m}$. Higher-order aberrations in retinal imaging of human can be compensated for by using adaptive optics. We demonstrate an adaptive optics system for *in vivo* imaging of fluorescent structures in the retina of a mouse, using a microelectromechanical system membrane mirror and a Shack–Hartmann wavefront sensor that detects fluorescent wavefront. © 2007 Optical Society of America
OCIS codes: 170.2520, 010.1080, 170.3880.

Studying the microscopic pathogenesis and progression of retinal disease in mice has until recently been confined to snapshots of histopathology after the animal has been sacrificed, which requires statistical studies of disease with large numbers of animals. *In vivo* retinal imaging is a powerful tool that allows following a single animal over time. A major problem with implementing this technique for visualization of single cells in the retina is the presence of aberrations in the rodent eye.^{1–3} In human retinal imaging and more recently in primates, adaptive optics (AO) has provided near-diffraction-limited imaging,^{4–10} but in the mouse this has not yet been achieved, although aberration measurements have been reported.³ Here we use an *in vivo* AO biomicroscope to compensate for aberrations in the mouse eye by monitoring the wavefront by using the fluorescent signal from cells. With improved resolution we have been able to image fluorescently labeled capillary vessels and dendrites of microglia cells.

Figure 1 shows the layout of the apparatus. For excitation of Evan's Blue fluorescence a 635 nm laser (Micro Laser Systems, Garden Grove, Calif.) was used. For excitation of green fluorescence protein (GFP) we use a 491 nm laser (Dual Calypso laser, Cobolt AB, Stockholm, Sweden). An entrance pupil is formed at the source and imaged on the AO element, a microelectromechanical system (MEMS) deformable mirror (DM) (Boston Micromachines Corp., Woburn, Mass.) The mirror consists of a square array of 144 actuators with a maximum stroke of $3.5\ \mu\text{m}$. The mirror was placed in a “two-pass” position, so that both the excitation and the fluorescent beams were reflected by the mirror. The pupil at the DM is imaged on a 36 facet polygon (Lincoln Laser Corp., Phoenix, Ariz.) that rotates at 480 revolutions per

second and provides the horizontal raster for the image. The pupil at the polygon is relayed to a galvometric mirror (GSI Lumonics, Billerica, Mass.) that provides the vertical scan for the image. This pupil is in turn imaged at the entrance pupil of a $50\times$, 0.5 NA long working distance (13 mm) microscope objective (Mitutoyo Corporation, Kanagawa, Japan). The mouse was mounted on a translation stage, for positioning the retina into the microscope's focal plane. Fluorescence is collected by the microscope objective and travels back through the system. After the fluo-

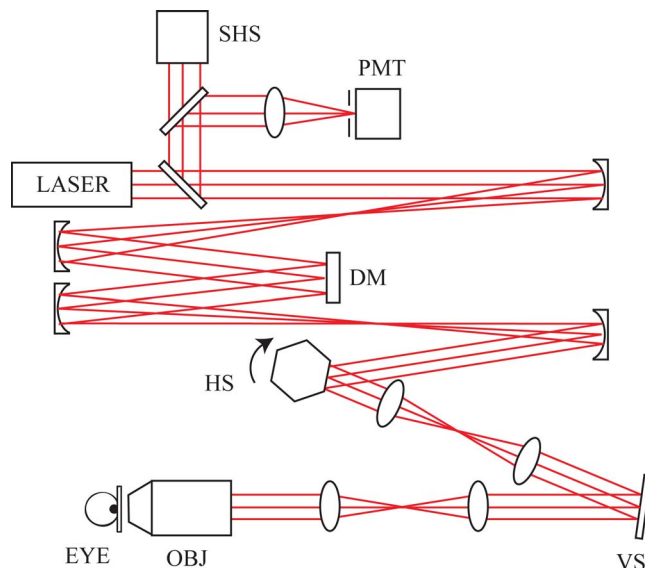


Fig. 1. (Color online) Experimental setup. DM, deformable mirror, SHWS, Shack–Hartmann wavefront sensor. PMT, photomultiplier tube for confocal detection of fluorescence, HS, polygon scanner for the horizontal scan. VS, galvanometric mirror for the vertical scan, OBJ, imaging objective, EYE, mouse eye sample.

rescent light is directed off the DM it is directed into a detection arm by a dichroic mirror. A beam splitter reflects some of that light to be focused through a confocal pinhole ($100\ \mu\text{m}$ diameter, which is $10\ \mu\text{m}$ imaged onto the retina) and detected by a PMT (R2896, Hamamatsu Photonics K. K., Hamamatsu City, Japan), while the transmitted light is collected by the Shack–Hartmann wavefront sensor (SHWS).

The AO system consists of a SHWS for wavefront measurement and a DM as the adaptive element. The SHWS, consisting of a CCD camera (UNIQ, Santa Clara, Calif.) and a lenslet array (Adaptive Optics Associates, Cambridge, Mass.), measures the wavefront of the fluorescent light at a plane conjugate to both the DM and the pupil of the microscope objective. A simple scattering target (here a piece of paper) in the focal plane of the microscope objective generates a calibration image in the SHWS. From this calibration image the control software builds an influence matrix between the action of individual DM actuators and the resulting SHWS pattern. The algorithm measures the SHWS spot deviation from the calibration image and then adjusts the mirror to minimize the spot deviations. While the SHWS measures the wavefront of the backscattered fluorescent light, the DM corrects the wavefront of both the forward- and backward-propagating beams. Thus, the two-pass design corrects the wavefront of the illumination and the fluorescence.

BALB/c, C57BL/6 or B6.129P-Cx3cr1^{tm1Litt}/J mice were anesthetized using a mixture of ketamin and xylazine in order to obtain long series of images and to facilitate the handling of the mice. All experimental procedures conformed to the ARVO Statement for the Use of Animals for Ophthalmic and Vision Research and were approved by the Massachusetts General Hospital (Subcommittee on Research Animal Care). Resident glial cells of the retina, microglia, express GFP in the transgenic B6.129P-Cx3cr1^{tm1Litt}/J mice. In either BALB/c or C57BL/6 mice, Evan's Blue (0.2–1%) was injected to label the vasculature. All mice received a drop of tropicamide 1% to dilate the pupil. The mice were placed on a heated microscope stage, and their eyes were covered with a lubricating agent (Methocel). A glass coverslip was positioned on the anterior surface of the cornea for visualization. The combination of the flat coverslip and microscope objective prevented the cornea from drying and nulled the refractive power of the cornea. Power levels of 1 and 0.2 mW at 635 and 491 nm, respectively, entered the eye. We estimated that our field of view of 0.5 mm square. These values are below the maximum permissible exposure for humans with exposure times less than 3 min.¹¹

In vivo images of Evans Blue labeled retinal blood vessels are shown in Fig. 2 along with the measured SHWS spot shifts superimposed on the calculated wavefront. All images are averages of 30 coregistered frames. The contrast of Figs. 2(a) and 2(c) was adjusted by the same criteria with ImageJ for display purposes.¹² To compute the wavefront, the slope displacement data were fitted to the OSA Standard Zernikes.¹² Comparing Figs. 2(c) and 2(a), see the ef-

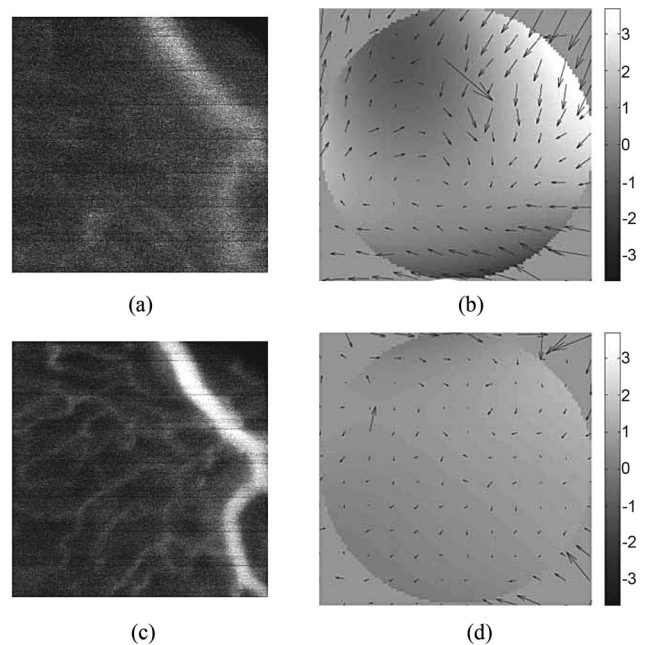


Fig. 2. *In vivo* images of retinal blood vessels injected with an Evan's Blue solution and measured SHWS spot displacements (arrows) with calculated wavefront (gray-scale image). The pupil at the SHWS is 4 mm across, and lenslets are $300\ \mu\text{m}$ in diameter and have a 7 mm focal length. (a) Image without AO correction. (b) Wavefront measurements before AO correction. (c) Image with AO correction. (d) Wavefront measurements after AO correction. The wavefront scale bar represents -3 to $3\ \mu\text{m}$.

fect of the AO system when imaging the fluorescently labeled blood vessels. Capillaries become resolved with correction, the vessel edge becomes sharper, and the fluorescent signal also becomes brighter. With the AO system on, the measured spot displacement RMS value is reduced from $24.48\ \mu\text{m}$ [Fig. 2(b)] to $14.82\ \mu\text{m}$ [Fig. 2(d)].

In vivo images of GFP-labeled microglia cells in the retina are shown in Fig. 3. The contrast of Figs. 3(a) and 3(b) was adjusted by the same criteria with the ImageJ for display purposes.¹² The inlaid plots in Figs. 3(a) and 3(b) show the increase in image brightness and contrast of the unprocessed data as a result of wavefront correction. A measurement of the Michelson contrast was measured for the intensity plots and multiple locations on the image. With the AO correction the contrast was seen to improve by approximately 7%. For comparison with *in vivo* images, Fig. 3(c) provides an *ex vivo* flatmount image of the same retina, taken with the same microscope, that is diffraction limited. With the AO correction on, the dendrites of the microglia begin to be resolved. The RMS spot deviation is reduced from 48.39 to $39.32\ \mu\text{m}$. By comparing the images in Figs. 3(b) and 3(c), we see that the AO correction has provided an image that closely resembles the expected diffraction-limited result.

It would be desirable to measure the wavefront for AO correction using backscattered light, but this proved difficult in practice. This difficulty probably arises because the SHWS lenslets have a very high *f*-number and therefore detect the light from all reti-

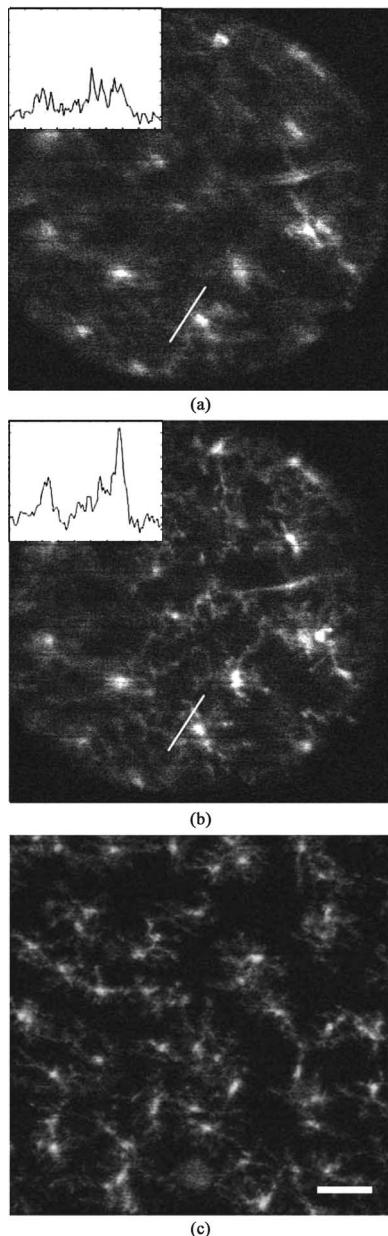


Fig. 3. *In vivo* images of GFP-labeled microglia in the retina. (a) Without AO correction. A line plot is given for the region of the image that corresponds to the white line. (b) With AO correction. In (a) and (b) pixel intensity from the original, unprocessed image along the white line is plotted on the same scale. (c) *Ex vivo* flat-mount image of the same retina. The dimension bar is $50\ \mu\text{m}$. Both inlayed line plots have the same x and y scale.

nal layers and the posterior surface of the lens, which is quite close to the retina of the mouse eye. Unlike the human eye, the mouse retina is thick ($200\ \mu\text{m}$) relative to its focal length (approximately $2\ \text{mm}$), and these reflections represent a mix of aberrations as well as very large blur circles. For the fluorescently labeled cells, the source for the SHWS measurements and the resulting confocal image is localized to specific layers and cells.

We have demonstrated the use of an adaptive optics system incorporated into a biomicroscope for im-

aging the mouse retina. Through the use of this system we have been able to visualize fluorescently labeled capillaries and dendrites of microglia cells. While partial correction was achieved, further improvement will require a deformable mirror with a longer stroke, or an external doubler.¹⁴ Nevertheless, the current system shows marked improvement in imaging. The ability to visualize retina at the cellular level is a great tool for studying the role of inflammation and/or apoptosis in the pathogenesis of diabetic retinopathy and age-related macular degeneration, diseases with increasing incidence and morbidity. *In vivo* imaging would allow temporal study of effects of therapies in the same animal and would greatly enhance new therapeutic strategies.

We thank Clemens Alt for helpful technical discussions. This research was supported by NIH grant EY-14106, and partial support for software development was also provided by EY-014375. Stephen Burns' current address, Indiana University, 800 East Atwater Avenue, Bloomington, Indiana 47405. D. Biss can be contacted at david.biss@schepens.harvard.edu.

References

1. M. Paques, M. Simonutti, M. J. Roux, S. Picaud, E. Levavassuer, C. Bellman, and J.-A. Sahel, *Vision Res.* **46**, 1336 (2006).
2. T. Higashide, I. Kawaguchi, S. Ohkubo, H. Takeda, and K. Sugiyama, *Invest. Ophthalmol. Visual Sci.* **47**, 2943 (2006).
3. E. García de la Cera, G. Rodríguez, L. Llorente, F. Schaeffel, and S. Marcos, *Vision Res.* **46**, 2546 (2006).
4. J. Liang, D. R. Williams, and D. Miller, *J. Opt. Soc. Am. A* **14**, 2884 (1997).
5. A. Roorda and D. R. Williams, *Nature* **397**, 520 (1999).
6. N. Doble, G. Yoon, L. Chen, P. Bierden, B. Singer, S. Olivier, and D. R. Williams, *Opt. Lett.* **27**, 1537 (2002).
7. A. Roorda, F. Romero-Borja, W. J. Donnelly III, H. Queener, T. J. Herbert, and M. C. W. Campbell, *Opt. Express* **10**, 405 (2006).
8. Y. Zhang, S. Poonja, and A. Roorda, *Opt. Lett.* **31**, 1268 (2006).
9. D. X. Hammer, R. D. Ferguson, C. E. Bigelow, N. V. Iftimia, T. E. Ustun, and S. A. Burns, *Opt. Express* **14**, 3354 (2006).
10. D. C. Gray, W. Merigan, J. I. Wolfing, B. P. Gee, J. Porter, A. Dubra, T. H. Twietmeyer, K. Ahamd, R. Tumar, E. Reinholz, and D. R. Williams, *Opt. Express* **14**, 7144 (2006).
11. F. C. Delori, R. H. Webb, and D. M. Sliney, "Maximum permissible exposures for ocular safety (ANSI 2000), with emphasis on ophthalmic devices," *J. Opt. Soc. A* (to be published).
12. W. S. Rasband, "ImageJ" National Institutes of Health, Bethesda, Maryland, USA, <http://rsb.info.nih.gov/ij/>, 1997–2006.
13. L. N. Thibos, R. A. Applegate, J. T. Schwiegerling, R. H. Webb, and V. S. T. Members, in *Vision Science and its Applications*, V. Lakshminarayanan, ed., Vol. 35 of OSA Trends in Optics and Photonics Series (Optical Society of America, 2000), pp. 232–244.
14. R. H. Webb, M. J. Albanese, Y. Zhou, T. Bifano, and S. A. Burns, *Appl. Opt.* **43**, 5330 (2004).